Hindawi
Advances in Materials Science and Engineering
Volume 2020, Article ID 9621591, 16 pages
https://doi.org/10.1155/2020/9621591

Research Article

Field Test and Numerical Analysis of In-Service Railway Bridge

Kang Liu[1], **Kai Hou**[1], **Zhongyu Fei**[1], **Ruoxi Shi**[2] and **Shaojie Wang**[1]

[1]*College of Water Conservancy and Civil Engineering, Shandong Agricultural University, Tai'an 271018, China*
[2]*College of Civil Engineering, Beijing Jiaotong University, Beijing 100044, China*

Correspondence should be addressed to Shaojie Wang; tumuwsj@sdau.edu.cn

Received 25 November 2019; Revised 29 December 2019; Accepted 8 January 2020; Published 8 February 2020

Academic Editor: Hiroshi Yoshihara

Field tests and numerical simulations are combined in this paper. Cross-sectional dimension measurements, dynamic performance tests, and forced vibration tests were performed on the NO·40 beam bridge of the Xin-Tai Railway. By comparing the test results with the specifications, the current service status of the bridge was evaluated, and the basis for subsequent correction and verification models was provided. A dynamic coupled finite element model of the passenger-freight-cable-track-bridge was established considering the degree of bridge damage (0%~50%) and the track irregularity, and the model simulation results for the Xin-Tai Railway NO·40 bridge were measured. The results are compared to verify the correctness of the model. The results show that the damage to the bridge will affect the vertical displacement response and the safety stability of the train. The vertical displacement response of the bridge midspan is twice that of the bridge performance. When the damage level of the bridge is 30%, the passenger and freight trains exceed the safety warning limit, which should cause concern.

1. Introduction

Reinforced concrete bridges are the backbone of bridge structures in China, especially in the railway network, and account for 83.4% of bridge structures. Passenger and freight railway consists of special passenger and freight train lines that concurrently operate and are designed to operate at speeds less than 200 km/h. Passenger and freight rail lines are extensively employed throughout the world. Although the majority of reinforced concrete bridges have entered the middle and final stages of their life cycles [1], replacing them on a large scale is not realistic. To ensure the safety of a train that crosses a bridge, correctly and effectively demonstrating its safety and stability is necessary.

The dynamic characteristics (natural frequency, mode, and damping ratio) of a structure can be estimated using current seismic codes or finite element models, which may significantly differ from the actual values [2]. Since running trains on old railway bridges cannot be interrupted, the incentive for vehicles that cross a bridge is adopted. The natural frequency, mode shape, and damping ratio of a bridge can be estimated by running a modal analysis [3]. The numerical model can be improved using a modal analysis and a comparison with experimental data [4, 5] to track the change in the dynamic parameters of a structure [6–11], which is a nondestructive technology for bridge detection.

In recent decades, research on the dynamic interaction of vehicle-rail bridges has increased and primarily focuses on the following aspects: (1) The dynamic response of trains in dangerous areas, such as road bridge transitions, curved bridges, and culvert transition zones [12–19]. (2) The dynamic performance of a train that passes through a bridge under external adverse influences, such as earthquake, wind and bridge skewness, or noise of composite bridge results [20–27]. However, few studies have addressed the dynamic response of passenger and freight trains that pass through old concrete railway bridges. Many scholars have done in-depth research on the field test of bridges. Li et al. [28] tested the three span continuous steel truss structure of the Baihe bridge in the Miyun reservoir, Beijing, and established the reliability evaluation method. Based on the field test, Morassi et al. [29] analysed and modified the finite element model of a concrete bridge with a complex structure type. Zanardo et al. [30] used a combination of field observations and structural dynamic tests to assess the condition of the bridge before and after CFRP reinforcement. The above work not

only shows the importance of bridge field tests but also indirectly provides guidance and theoretical support for this study.

In this paper, the innovation lies in that it not only emphasizes the safety of the bridge itself but also the safety of the train-track-bridge interaction system. This work not only evaluates the safety of the existing railway bridge based on the present conditions but also considers the future circumstances and forecasts the train operation safety of the bridge under different damage conditions. Using the predetermined information obtained from the field test, the model is modified, and a refined dynamic coupling finite element model of passenger and freight train ballasted track simply supported beam bridges is established. On the basis of the model, the safety and stability of a passenger and freight train crossing the bridge under different damage degrees are studied, and the safety criterion for the operating passenger and freight train is proposed.

2. Case and Measurement

2.1. Case: NO 40 Railway Bridge. The NO·40 Railway bridge near the village Zhitian overcomes the Mouwen River on the Xin-Tai Railway line, which starts from Linzi station of the Jiao-Ji Railway in the north and ends at Taishan station of the Jin-Pu Railway in the west. The bridge was built in 1972 and is a typical old reinforced concrete railway bridge. The spans of the bridge between the supports are 7×18 m. The height and width of the bridge beam, which is a simply supported beam, is 1.6 m and 3.9 m, respectively. Photos of the scene and detailed sections are presented in Figure 1.

2.2. Measurement Profile. The static and dynamic load test was performed on November 11, 2018. The main objective was to ascertain the effect of existing traffic on the bridge to verify the safety of the railroad and the compliance between the measured quantities and the calculated quantities determined on the finite element model. This verification can be applied for finite element model updating. Figure 2 shows the dynamic performance test of the NO·40 bridge of the Xin-Tai Railway and the layout of the train bridge pulsation test.

Measuring points for bridge: a total of 5 measuring points is established, which were arranged at the beam support, 1/4 and 1/2; a detailed layout of the bridge measuring points is presented in Figure 2. The dynamic displacement and longitudinal and transverse modes of the beam body are measured. The displacement sensor is arranged in the middle of the beam span to test the dynamic displacement of the beam body when the train passes through the bridge. The acceleration sensor is arranged in the middle span, support, and quarter span of the beam body to test the transverse and vertical amplitude, acceleration, and other parameters of the beam body.

To measure the natural vibration frequency in the bridge structure, the magnetoelectric speed sensor 941B was employed. The 941B magnetoelectric speed sensor is a multifunctional instrument for ultralow frequency vibration measurement developed by Institute of Engineering Mechanics, China Earthquake Administration. It has the following advantages: (1) One machine with multiple functions: it can directly measure acceleration or velocity, and can measure displacement when it is connected with amplifier. (2) Simultaneous measurement of multiple physical quantities: passive servo vibration sensor with multiparameter measurement model can realize acceleration and velocity direct measurement. (3) Easy to use: the vibration pickup does not need power supply and zero adjustment. (4) Excellent performance: because of the use of passive servo feedback technology, it can achieve ultralow-frequency large displacement vibration measurement. (5) Wide frequency band, high resolution, large dynamic range, good impact resistance, suitable for transportation, and can be directly connected with various data acquisition systems. Natural incentives were employed for measurement. The vibration collectors pick up the environmental vibration acceleration response of the bridge and transmit the signal to the data acquisition analyser. The signal is processed by the computer system and analysis software and displayed in the plotter. The sampling frequency is 200 Hz. The obtained data are processed by FIR low-pass digital filter, and the passband cutoff frequency is 80 Hz.

In the field test, the passenger group of the Xin-Tai Railway was measured for two trips with a maximum speed of 59.9 km/h, and the freight group was measured for two trips with a maximum speed of 59.8 km/h. The passenger group includes 1 DF11 headstock and 4 YZ25B carriages. The freight group is divided into two types: empty freight trains and loaded freight trains. The empty freight train has 1 DF11 headstock and 46 C70 carriages, and the loaded freight trains have 1 DF11 headstock and 56 C70 carriages. Figure 3 details the measured trains.

2.3. Analysis of Measurement Data

2.3.1. Railway Bridges Forced Vibration Measurement. The vibration acceleration of the bridge deck should be controlled to ensure the stability of the line and the structure of the bridge. With the action of the trains, the maximum value of the measured vertical acceleration of the beam body is 3.64 m/s^2, which satisfies the requirement of the 5.0 m/s^2 limit value of the ballast track in the China code [31].

When the DF11 locomotive passes through the bridge at about 60 km/h, Figure 4 shows the acceleration response measured by the I, II, and III measuring points on the bridge when the three trains pass the bridge. According to the measured values, the vertical acceleration of all parts of the beam body of the same type of vehicle that passes through the bridge is equal and small. The maximum vertical acceleration is 0.500 m/s^2, and the maximum transverse acceleration is 0.547 m/s^2. The maximum vertical acceleration is 0.610 m/s^2, and the maximum lateral acceleration is 0.644 m/s^2 when the locomotive passes through the bridge. The empty freight train through the bridge beam body undergoes a vertical acceleration change near 0.748 m/s^2, a lateral acceleration change near 0.618 m/s^2, a maximum vertical acceleration of 1.998 m/s^2, and a

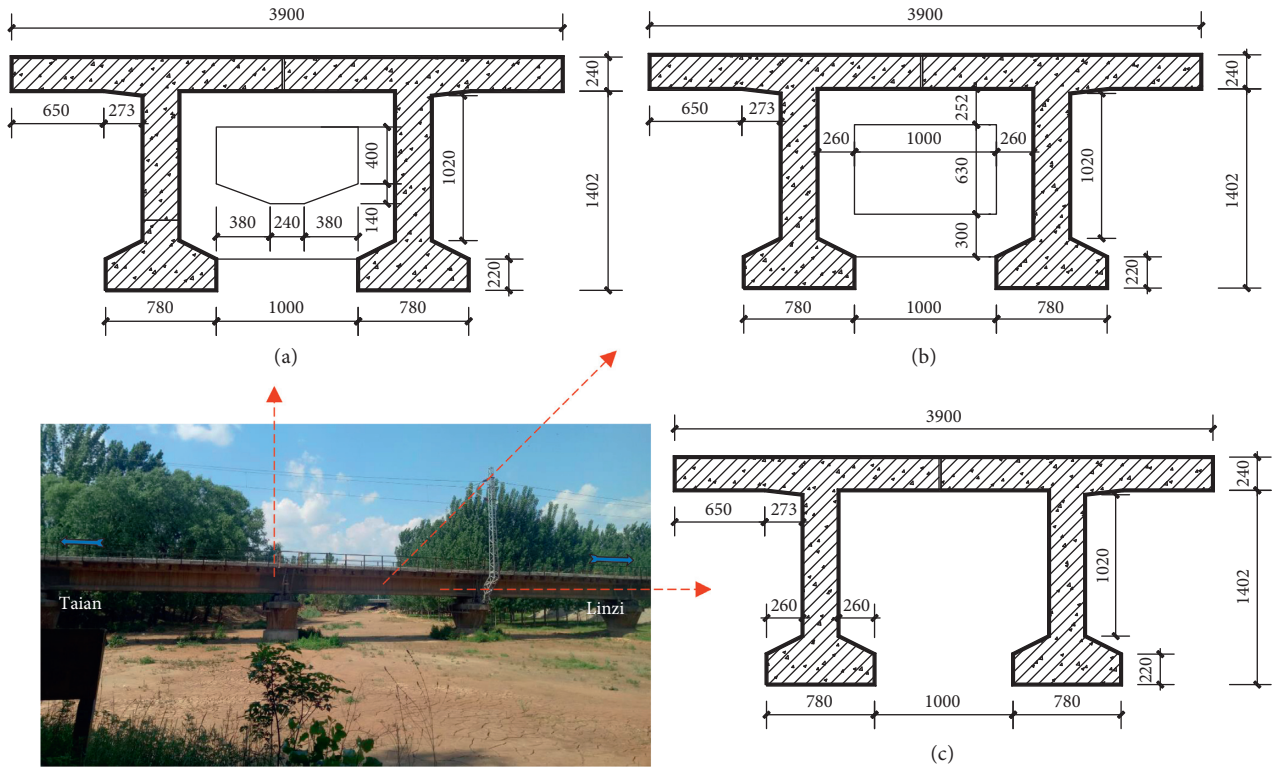

Figure 1: Xin-Tai Railway NO·40 bridge and side elevation of the bridge (units: mm). (a) Support cross section, (b) 1/2 and 1/4 cross section, and (c) another cross section.

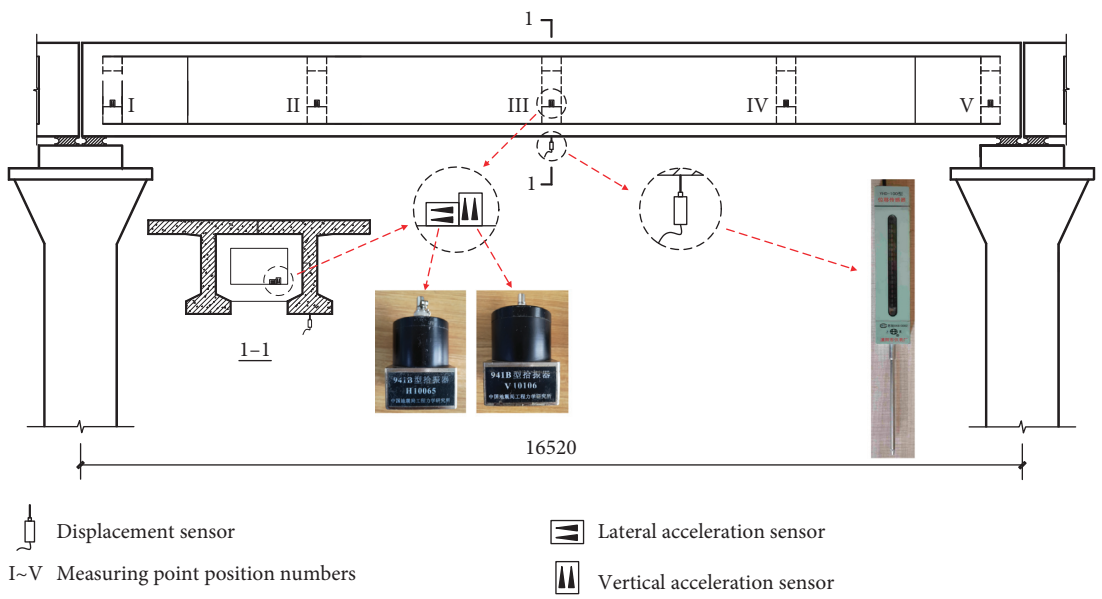

Figure 2: Measuring point layout (units: mm).

maximum lateral acceleration of 0.929 m/s^2. When the car travels through the bridge beam body, the vertical acceleration is 0.929 m/s^2 and the maximum lateral acceleration is 1.432 m/s^2. The freight train through the bridge beam body undergoes a vertical acceleration change near 1.725 m/s^2, a lateral acceleration change near 1.957 m/s^2, a maximum vertical acceleration of 3.638 m/s^2, and a maximum lateral acceleration of 3.830 m/s^2. The acceleration at the front by the beam body is higher than that of the model. When the last carriage through the beam body encounters a period of turbulence, analysts suggest that the bridge bearings have a certain damping. The maximum vertical acceleration of the beam body is higher than that of other vehicle models when the carrying truck passes through the bridge.

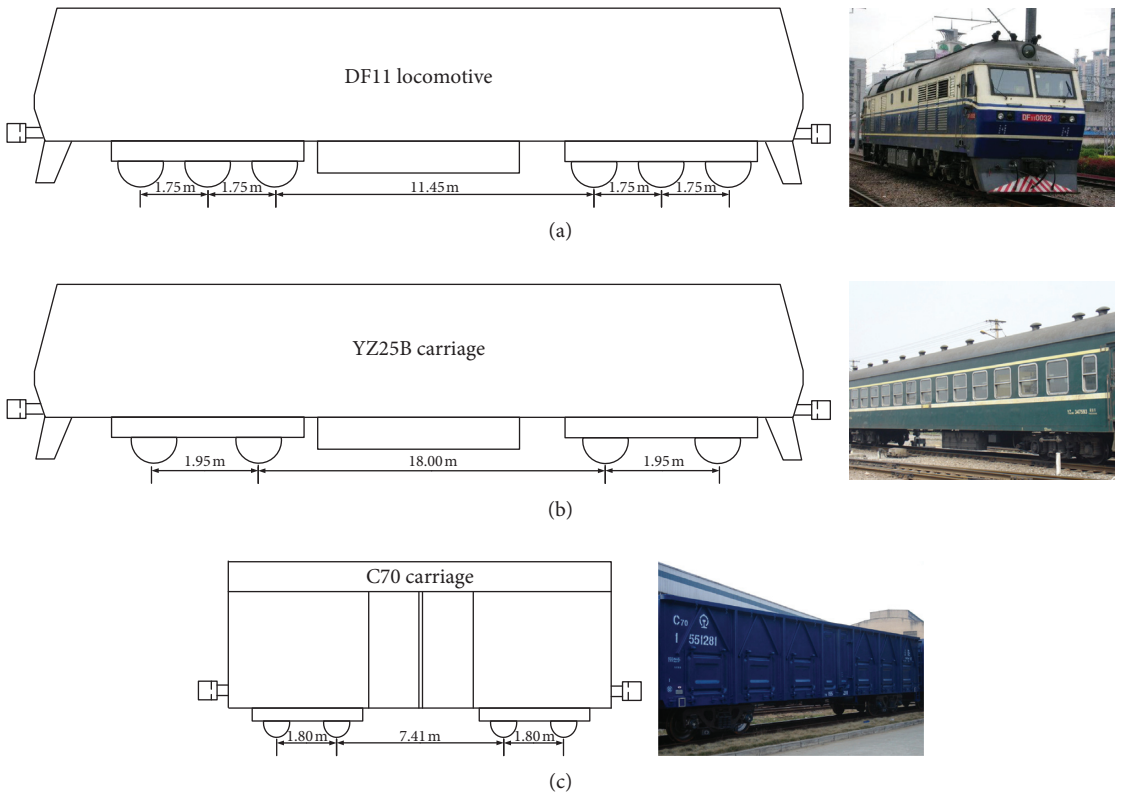

Figure 3: Test train type. (a) DF11 locomotive model and photo. (b) YZ25B carriage model of the passenger train and photo. (c) C70 carriage model of the freight train and photo.

Controlling the vibration acceleration of the bridge deck is a necessary measure to ensure the stability of the bridge deck structure. With the action of passenger trains and vans, the maximum vertical vibration acceleration of the beam varies from 0.290 to 1.990 m/s^2, both of which satisfy the requirements of the maximum vertical vibration acceleration and the minimum vertical vibration acceleration of 3.500 m/s^2 for the ballasted track in the specification. With the action of trucks, the measured vertical vibration acceleration of the beam is 3.638 m/s^2, and the local short-term acceleration is higher than 3.500 m/s^2, which is worthy of follow-up attention in the current operating state.

Figure 5 shows the maximum response deflection of the bridge measured when passenger and freight trains pass. As shown in Figure 5(a), when the passenger train passes the bridge at 59.9 km/h, the vertical deflection of the bridge beam changes near 0.2 mm when the carriage passes, the maximum vertical deflection is −0.41 mm, and the bridge beam passes when the front of the vehicle passes. The maximum vertical deflection is −0.93 mm. As shown in Figure 5(b), when the truck-less car passes through the bridge beam, the vertical deflection changes near −0.24 mm and the maximum vertical deflection is −0.32 mm. The maximum vertical deflection is −1.00 mm; as shown in Figure 5(c), when the freight car passes through the bridge beam, the vertical deflection varies near −0.81 mm and the maximum vertical deflection is −1.07 mm. The maximum vertical deflection is −0.99 mm. When the loaded truck passes, the maximum vertical deflection of the beam body is larger than that of other test models. According to the analysis, this finding is attributed to the heavy axle weight of the loaded truck. As shown in Figure 5, the weight of the head of the passenger train and the empty freight train is significantly larger than that of the train. The maximum span ratio of the bridge beam when crossing the bridge appears in the front part, the weight of the freight train is heavier than that of the front, and the maximum span ratio will appear in the corresponding compartment part. The measured results are less than the limit value of the specification, which indicates that the bridge has sufficient vertical stiffness.

2.3.2. Railway Bridges Natural Vibration Frequency. The vibration of the bridge was measured by ten piezoelectric acceleration transducers under environment excitation. By the arrangement of the sensor on the bridge, the NO·40 bridge was measured in the conditions of the natural environment excitation frequency domain curve, the lateral frequency domain and corresponding vibration mode are shown in Figure 6(a), and the vertical frequency domain and corresponding vibration mode diagram are shown in Figure 6(b). In the process diagram, the abscissa represents frequency, and the ordinate represents the speed signal amplitude. The vertical first order is 15.625 Hz (damping ratio is 0.983%). The horizontal first order is 11.523 Hz (damping ratio is 0.442%), which is higher than the limit of 5.625 Hz in the code in China, which shows that the bridge body has excellent lateral stiffness in the normal operation of passenger and freight trains.

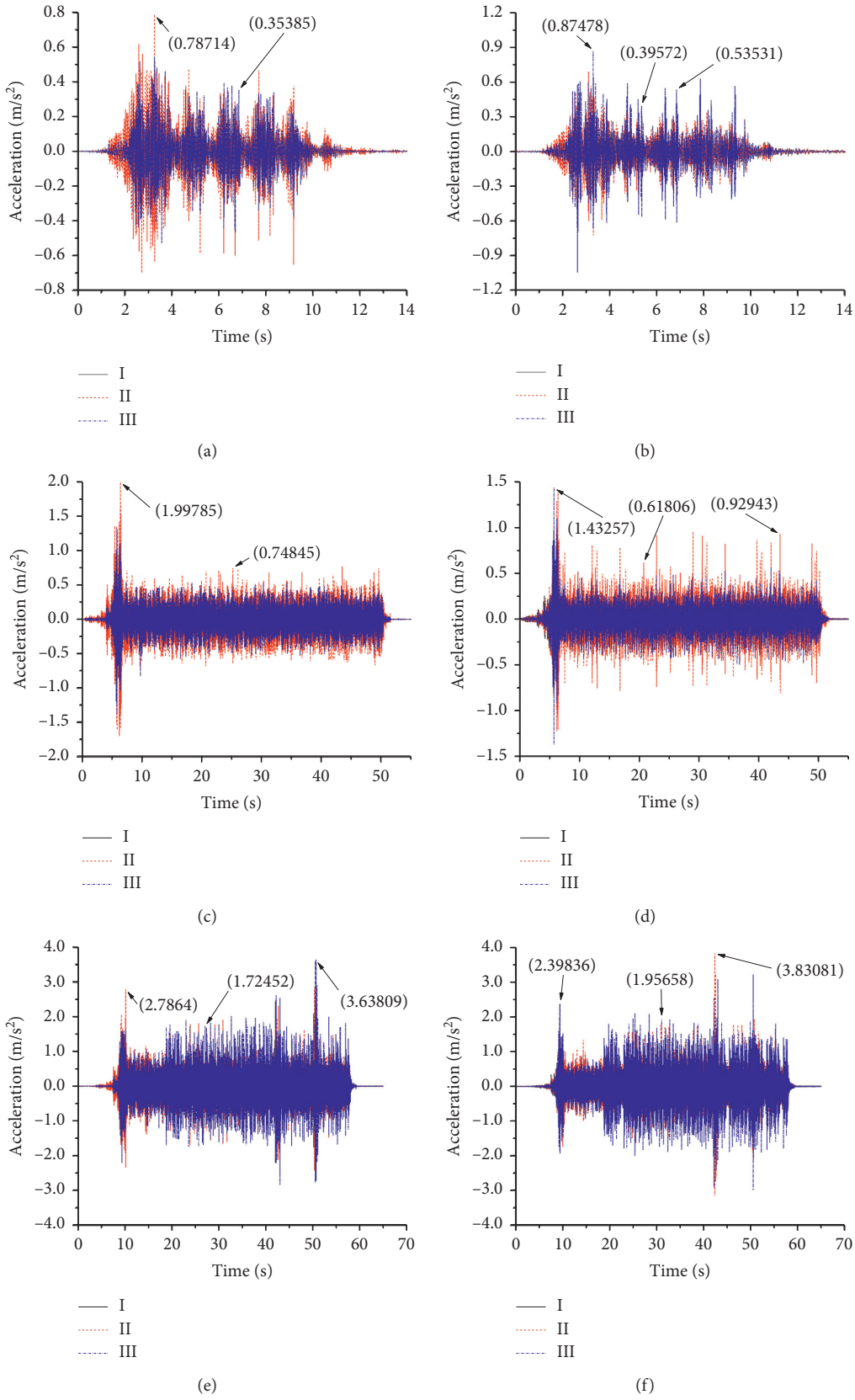

Figure 4: Acceleration response of the bridge with a passing vehicle. (a) Passenger train vertical. (b) Passenger train lateral. (c) Freight trains (empty) vertical. (d) Freight trains (empty) lateral. (e) Freight trains (cargos) vertical. (f) Freight trains (cargos) lateral.

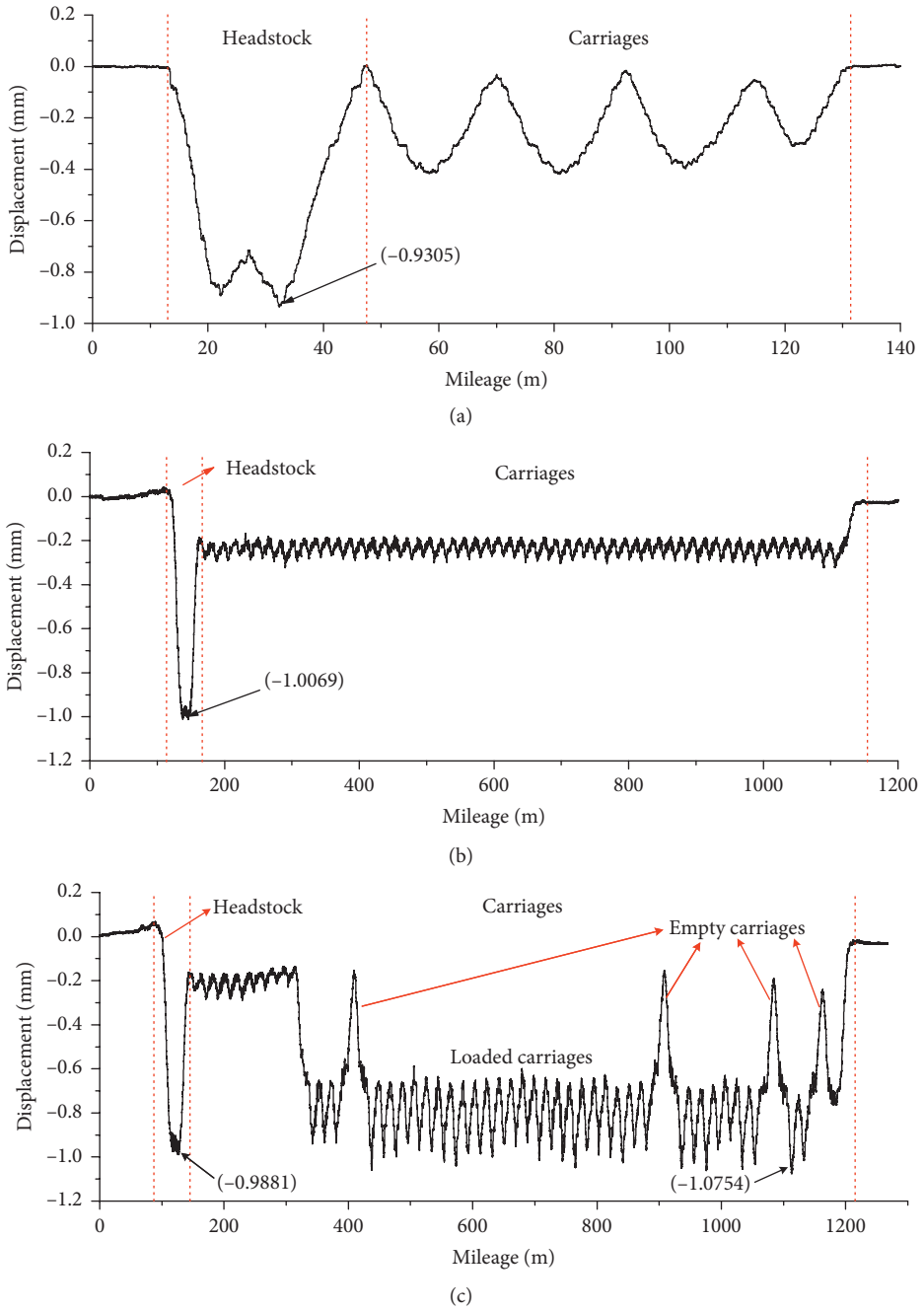

Figure 5: Measured velocity time history curve. (a) Passenger train. (b) Freight trains (empty). (c) Freight trains (cargos).

3. Dynamic Model of Train-Track-Bridge with the Performance Degradation

This section provides a concise and precise description of the experimental results, their interpretation, and the experimental conclusions.

3.1. Physical Model

3.1.1. Train Model. The subsystem model of the freight trains is divided into two parts: DF11 locomotive and C70 carriage. The subsystem model of the passenger train is divided into two parts: DF11 locomotive and YZ25B carriage. In the model, the C70 carriage of the freight train and the YZ25B carriage of the passenger train have the same physical model as shown in Figure 7, but there are differences in the locomotive mass and wheelbase (as shown in Table 1). The subsystem model of the freight trains is divided into two parts: the DF11 locomotive and C70 carriage. The DF11 locomotive is a six-axle locomotive (C0-C0 axle type) model; it consists of a car body, two frames, six wheelsets, a total of nine rigid bodies, and a suspension system of one- and two-system suspension systems. Similar to the DF11 locomotive model, the C70 carriage model is a four-axle locomotive model that consists of a car body, two frames, four

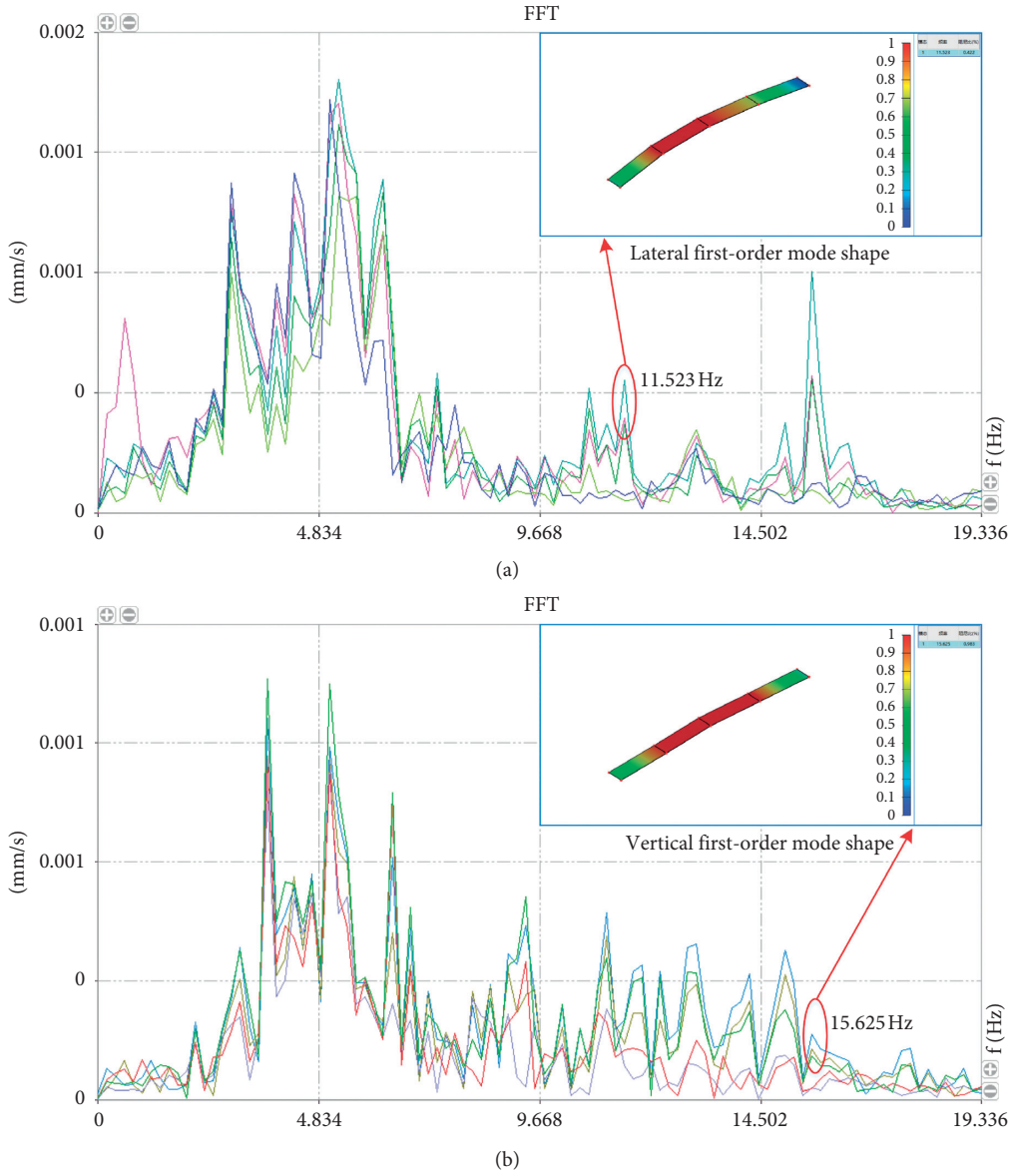

Figure 6: Frequency domain and corresponding mode shapes. (a) Lateral and (b) vertical.

wheelsets, a total of seven rigid bodies, and a two-system suspension system. The degrees of freedom of each rigid body are equivalent to those of the locomotive. The vehicle body and bogie consider the degrees of freedom of sinking and floating, the wheel pair considers the degrees of freedom of sinking and floating, and the remaining degrees of freedom are restrained. The dynamic interaction between the cars is not considered. The steel rail adopts the long track embedded ballast-less track, whose vibration is primarily reflected by the rail vibration. The relationship model between the lower support of the track and the bridge is simulated by the spring and damping element. The finite element method is used to model the bridge structure, and Rayleigh proportional damping is employed in the dynamic analysis.

3.1.2. Track Model. The ballast track, which consists of the rail, fastener, rail pad, sleeper, and ballast, is modelled as a discretely supported three-layer system that considers the degrees of the rail, the sleeper, and the ballast. The rail is treated as a continuous Bernoulli–Euler beam, which is supported by discrete points of springs and dampers that represent the elasticity and damping of the rail pad. The sleeper is represented by a rigid beam, and the vertical is considered. The ballast bed is replaced with the equivalent rigid ballast body, in which only the vertical motion is taken into account. The Hertz elastic contact model is used to calculate the track irregularity, and the superposition caused by the change in the beam shape is considered.

3.1.3. Bridge Model. As shown in Figure 8, a finite element model of a simply supported beam bridge with a span of 16 m is established. The finite element model of the bridge considers the three sections of the Xin-Tai Railway NO 40 bridge. Three types of beam sections are established in the

model: the polygonal section at the beam support and the 1/2 and 1/4 sections of the beam. Other T sections at the cross section are considered. The pier is a circular pier with the following dimensions: the beam 188 space beam unit is used for the upper beam body and the pier of the bridge. The horizontal and vertical stiffness of the rubber plate bearing is modified between the bridge beam body and the bridge pier. The parameter values are the concrete elastic modulus $E = 3357.95$ MPa, density $\rho = 2200.3\,\text{kg/m}^3$, bearing vertical stiffness $K_v = 1.16 \times 10^{11}$ N/m, and lateral stiffness $K_h = 4.77 \times 10^{10}$ N/m.

In the model of the bridges, the beam 188 elements are used for the simply supported beam bridges and the variable section circular piers of the three cross-section types. The proportional damping is used for the dynamic analysis of the three types of bridge beam bodies, namely, $C = \alpha M + \beta K$, where C is the proportional damping, M is the mass matrix, and K is the stiffness matrix. The mass damping coefficient and the stiffness damping coefficient are determined by equations (1) and (2).

$$\alpha = \frac{2\xi}{\omega_i + \omega_j}\omega_i\omega_j, \tag{1}$$

$$\beta = \frac{2\xi}{\omega_i + \omega_j}, \tag{2}$$

where ω_i and ω_j are the i-th order reference frequency and j-th order reference frequency, respectively, of the bridge structure; and ξ is the structural damping ratio that depends on the type of the material. In the analysis of train-track-bridge coupling vibration, the existing research results suggest [32] the use of the following parameters to calculate the Rayleigh damping coefficient: a structural damping ratio of 2% for the concrete structure; ω_i is set to the basic frequency of bridge structure ω_1, which is determined by modal analysis, $\omega_i = \omega_1 = 9.773$ Hz; ω_j is suggested to take the maximum excitation frequency generated by the track geometric irregularity, $\omega_j = \omega_f = V_{\max}/\lambda = 60/(3.6 \times 1.524)$ Hz $= 10.936$ Hz, where $V_{\max}$ is the maximum speed of the train crossing the bridge and λ is the minimum wavelength of track geometric irregularities. If formulas (1) and (2) are combined, $\alpha = 0.20644$ and $\beta = 0.0019315$, respectively.

3.2. Performance Degradation Model. The equation of the simple support beam fundamental frequency (ω) is [33]

$$\omega_n = \frac{n^2\pi^2}{l^2}\sqrt{\frac{EI}{\overline{m}}}, \quad n = 1, 2, \ldots, \tag{3}$$

where ω is the angular frequency, E is Young's modulus of elasticity, I is the moment of inertia, l is the mass per unit length, l is the beam length, and n is the order of the mode. Without damaging the girder of the bridge, the beam's section length and mass did not change; that is l, I, and $\overline{m}$ did not change. Therefore, the frequency change before and after the bridge measurement is attributed to the change in elastic modulus E. For simply supported beams, the degree of damage can be measured by the change in elastic modulus. The larger the degree of the damage, the larger the decrease in the frequency and elastic modulus.

3.3. Track Irregularity Model. The random irregularity of orbits is generated by the American orbital spectrum (Grade-3). In this study, only high and low irregularity are considered, and the inverse Fourier transform method is used to generate time-domain samples with high and low irregularity. Aimed at orbit irregularity, the American orbit spectrum is briefly described as follows:

$$S_v(\Omega) = \frac{kA_v\Omega_c^2}{\Omega^2\left(\Omega^2 + \Omega_c^2\right)}. \tag{4}$$

$S_v(\Omega)$ is the power spectral density for track irregularity (cm^2/(rad/m), Ω is the spatial frequency (rad/m), A_v is the roughness constant (cm^2·rad/m), Ω_c is the truncation frequency (rad/m), and k is a safety factor. Figure 7(b) shows the generated track irregularity.

3.4. Finite Element Model. The numerical model of the interaction system between a passenger and freight train-ballast-track and a bridge based on the measured bridge is established with the finite element software ANSYS, as shown in Figure 8. The finite element model of the passenger train-ballast-track and bridge consists of 5,218 nodes and 7,871 elements (total length is 320 m), and the finite element model of the freight train-ballast-track and bridge consists of 7,345 nodes and 10,913 elements (total length is 380 m).

The passenger train model consists of 1 headstock and 4 passenger carriages, the length of the headstock is 21.28 m, the passenger carriage measured from the first wheelset to the final set is 25.5 m, and the total length is 120.18 m. The freight train model consists of 1 headstock and 11 freight carriages, the length of the freight car measured from the first wheelset to the final set is 12.49 m, and the total length is 164.77 m. A total of 5,549 elements, including beam, pier, and rail, are modelled. Detailed information about each vehicle is listed in Table 1. In the three-dimensional finite element model of the train, all vehicles are regarded as multiple rigid body systems.

The track type investigated in this study is the ballast track, which consists of a steel track, fastener, reinforced concrete sleeper, and track bed. In the ballast track, the steel track, sleeper, and track bed will undergo vibration. The infinite length Euler beam is used to discretize the rail, and the linear spring and damping element are used to simulate the vertical and lateral restraints on the rail at the node position that corresponds to the fastener. The sleeper is regarded as a rigid body and its vertical, lateral motion and rotational freedom are considered. The the rail and the sleeper and the sleeper and the rail bed are connected by linear spring and viscous damping. The track bed is discretized into mass blocks according to the actual distance between sleepers, and its vertical vibration is considered. The sleeper is connected to the ballast, the ballast is connected to the roadbed by linear spring and viscous damping, and the

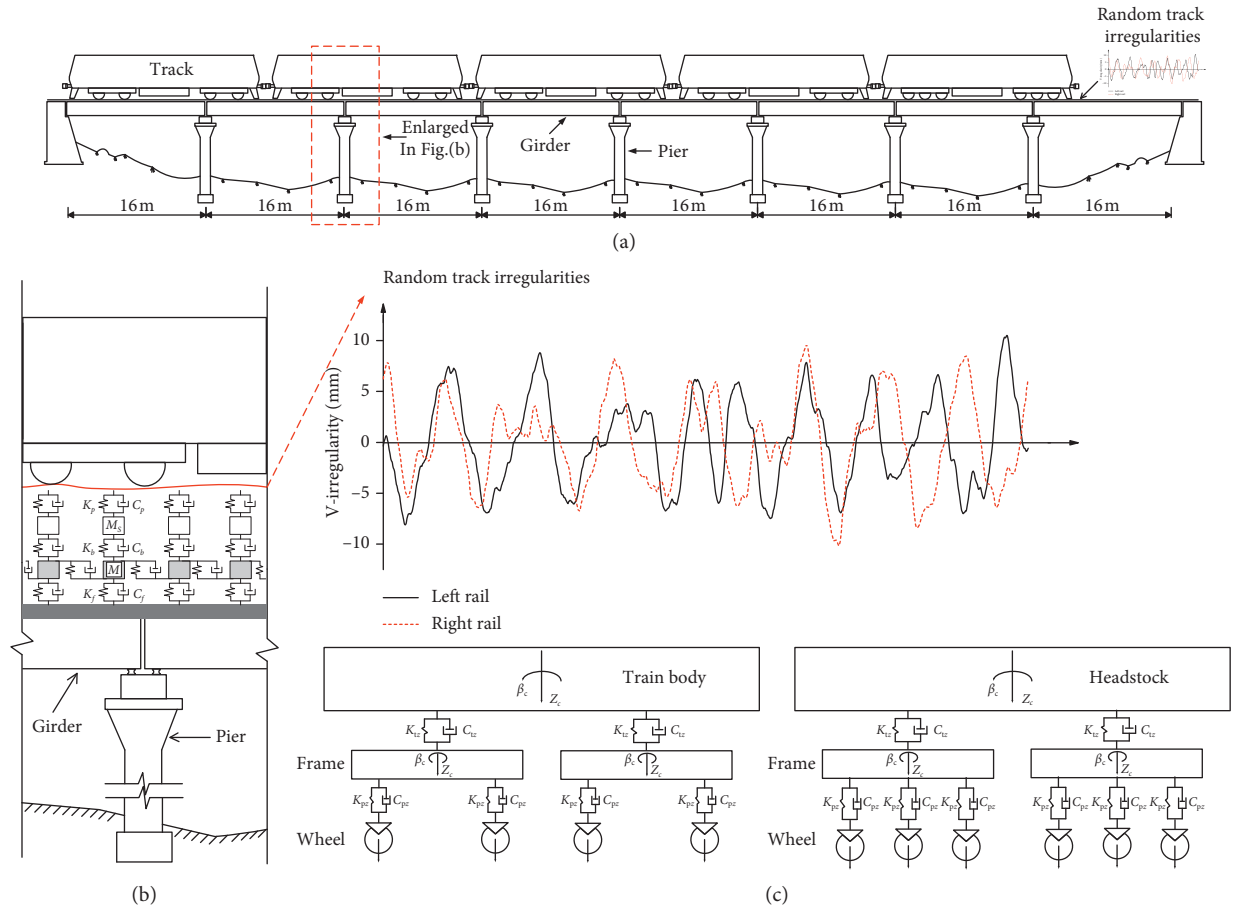

Figure 7: Physical model of train–track–bridge interaction system. (a) Total frontal view. (b) Detailed view of one section highlighted with a dashed box in (a). (c) Vehicle dynamics model diagram.

Table 1: Model parameters of locomotive.

Parameter	Value
Mass of car body (headstock) (ton)	141.4
Mass of car body (type 22 passenger car) (ton)	45.5
Mass of car body (freight car) (ton)	23
Mass of bogie (ton)	3.2
Mass of wheel axle (ton)	2.4
K_{py} (N/m)	3×10^6
C_{py} (N·s/m)	2.12×10^6
K_{pz} (N/m)	1.04×10^6
C_{pz} (N·s/m)	5.0×10^3
K_{ty} (N/m)	0.24×10^6
C_{ty} (N·s/m)	3.0×10^4
K_{tz} (N/m)	1.51×10^6
C_{tz} (N·s/m)	0.4×10^6
L_c (headstock) (m)	20.15
L_c (passenger car) (m)	23.60
L_c (freight car) (m)	11.40
L_t (m)	2.5
d_{sk} (m)	1.956
d_{wk} (m)	1.496
H_{cb} (m)	1.7
H_{bt} (m)	0.14
H_{tw} (m)	0.28

engagement of the ballast is simulated by the shear stiffness and damping between the mass blocks of the ballast. The ballast track parameters are listed in Table 2.

Several commercial FEM tools enable contact analysis. To analyse the wheel-track contact, wheel-rail force, and offload factor, the node-to-surface contact elements in ANSYS (CONTA175 and TARGE169) are used. The basis of this method is the Hertz contact theory. The solution is obtained using a step-by-step Newmark-β method with the time step $\Delta t = 0.001$ s, and the dynamic responses of the vehicle and bridge can be obtained in the time domain [34, 35].

3.5. Model Updating and Validation

3.5.1. Analysis of Vibration Characteristics of Railway Bridge Beam. According to equation (3), substitute $I = 0.2316\ \text{m}^4$, $l = 16$ m, and $\overline{m} = 4734.7$ kg/m.

Obtain the equation: $15.625 = (\pi/16)^2(\sqrt{E\times 0.2316/4734.7})$; solution of $E = 3357.95$ MPa.

The inaccuracy of the finite element model is derived from three aspects: model structure error, model order error,

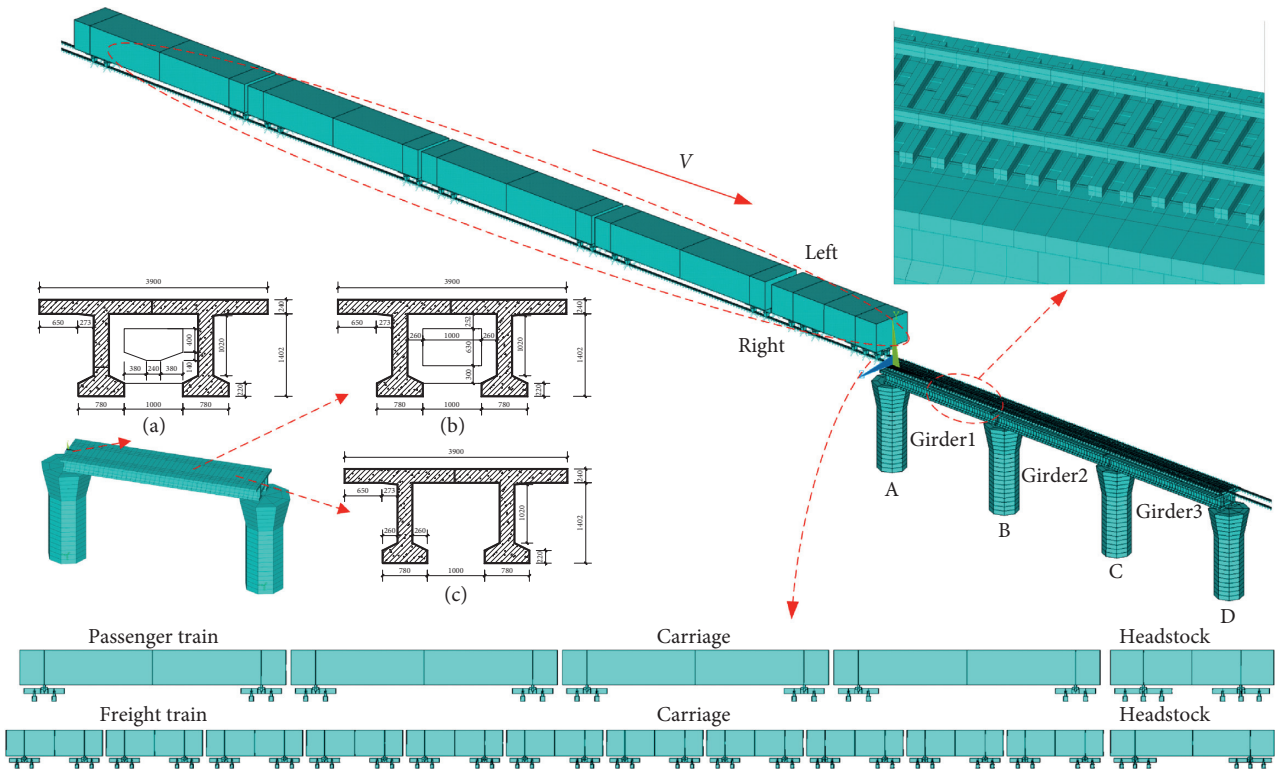

Figure 8: FEM models of the train–track–bridge interaction system. (a) Support sections. (b) 1/2 and 1/4 sections. (c) Other sections.

Table 2: Ballast modelling parameters.

Parameter	Value
With rail cushion stiffness (N/m)	1.0×10^{8}
With rail cushion damping ratio (N·s/m)	7.5×10^{4}
Ballast bed density (kg/m^3)	1.8×10^{3}
Ballast bed modulus (Pa)	1.1×10^{8}
Ballast bed damping coefficient (N·s/m)	5.88×10^{4}
Ballast bed shear damping (N·s/m)	8.0×10^{4}
Ballast bed thickness (m)	0.45
Roadbed modulus (Pa)	9.0×10^{7}
Roadbed damping coefficient (N·s/m)	3.115×10^{4}

and model parameter error. The error in the modulus parameter is the main factor of the finite element error in this model. The errors in the model parameters are usually caused by imprecise material, geometric parameters, and joint boundary condition estimation. In this paper, the boundary conditions are assumed to be accurate when the finite element model parameters of bridges are modified. The finite element model of a bridge crane is analysed, which is primarily based on the imprecise modelling of the following parts. First, the connection between the cross-beam and two T beams is considered. Second, ballasted track and other ancillary facilities on the bridge are not considered.

After analysing the eigenvalue sensitivity of the structural parameters, unless sensitive parameters are present, design variables are determined from the groups of parameters to be modified, that is,

$$X = [prxy, K_h, K_v]. \tag{5}$$

State variable,

$$\begin{aligned} A &= 11.523 - f_1, \\ B &= 11.625 - f_2, \end{aligned} \tag{6}$$

where K_h is the horizontal elastic modulus of the bridge support, K_v is the vertical elastic modulus of the bridge support, and f_1 and f_2 are the first-order frequency of the bridge and second-order frequency of the bridge, respectively. The mathematical model for optimizing the iterative process is expressed as follows:

Minimum value,

$$f_{\text{object}} = \left(\frac{A}{11.523}\right)^2 + \left(\frac{B}{15.625}\right)^2. \tag{7}$$

Constraint condition

$$\begin{cases} 0.1 \le prxy \le 0.5, \\ 4.5\times10^{10} \le K_y \le 5.0\times10^{10}, \\ 1.0\times10^{11} \le K_z \le 1.1\times10^{11}, \\ |A, B| \le 0.05. \end{cases} \tag{8}$$

The optimization results are K_h is 4.776×10^{10} (N/m^2) and K_v is 1.161×10^{11} (N/m^2).

Using the zero-order optimization method of ANSYS, the modal parameters obtained from the actual test are considered to be the expected modal parameters and the optimal modal parameters are calculated. The simulation value of the first horizontal order is 11.918 Hz, the relative error with the measured value is 3.31%, the simulation value

of the first vertical order is 15.027 Hz, and the relative error with the measured value is −3.83%, which indicates that the modelling parameters can better simulate the real bridge. Thus, the calculated and corrected parameters are correct.

3.5.2. Field Measurement and Comparison with Calculation Results. To ensure the correctness of the following analysis and the driving safety criterion, this section will verify the correctness of the passenger-freight train-rail-bridge modelling in this paper. First, the model parameters of the passenger-freight train-rail-bridge model in this paper are confirmed to be accurate before the simulation calculation. Second, the calculation results of the vehicle-rail-bridge model in this paper are compared with the results obtained from the actual test to ensure that the solution results are compared when the parameters of the established model are identical and to verify the correctness of the research model in this paper. In this paper, the measured dynamic deflection of the midspan bridge of the Xin-Tai Railway NO·40 bridge in actual operation is selected for comparison.

Figure 9 shows the comparison between the actual test results and the simulation results of the dynamic deflection measured in the midspan of the bridge when the passenger train on Xin-Tai railway runs at a speed of 60 km/h.

As shown in Figure 9, with the exception of the difference between the simulation results and the measured results of the midspan deflection of the passenger train that passes the bridge, the error of the other carriages is small and within 1%.

4. Simulation of Passenger and Freight Trains with Performance Damage of Bridge

4.1. Evaluation of Bridge Linear Change in Case of Damage. In this study, the damage of the whole bridge is considered. Based on continuum mechanics, it can be seen that the local damage of the bridge cannot fully reflect the overall state, and the overall damage of the bridge will eventually affect the operation by means of the deformation of the bridge, so it is feasible to consider the damage of the whole bridge beam in the model. The Lemaitre theory [36, 37] shows that the classical elastic modulus method can fully and completely describe the damage. In this paper, the damage degree of the bridge performance is defined as 0% in the in situ test, and further damage is defined as 10%–50% in increments of 10%, which corresponds to the bridge elastic modulus of the same degree of reduction.

Figure 10(a)–10(c) shows the displacement of the passenger train, freight train without freight, and freight train with freight when passing through the bridge with different degrees of damage. When the passenger train passes the bridge with 0% damage, the maximum displacement is 0.986 mm; when the bridge incurs 50% damage, the maximum displacement is 1.928 mm. When the freight train passes the bridge with 0% damage, the maximum displacement is 1.553 mm; when the bridge incurs 50% damage, the maximum displacement is 3.030 mm. When the freight train passes through the bridge with 0% damage, the maximum displacement is 1.199 mm; when the bridge incurs 50% damage, the maximum displacement is 2.364 mm. When the performance is degraded by 50%, the vertical displacement of the bridge is approximately twice as large as when the performance is degraded by 0%. As shown in Figure 10, the maximum vertical displacement exponentially increases with the damage to the bridge performance.

4.2. Safety of Passenger and Freight Train Running on Bridges with Performance Damage of Bridge. This section provides an analysis of the offload factor when a passenger train or freight train is rolling on various levels of the performance damage of the bridge at 0–50% in increments of 10%. Figure 11(a) depicts the maximum offload factors of the passenger train obtained for the different level performance damage of the bridge.

As shown in Figure 11, when the bridge is not damaged, the maximum wheel load shedding rate appears in the freight train compartment. The maximum wheel load shedding rate of the car and the front is 0.583 and 0.555, respectively. The difference between the two values is 0.028. Less than the standard limit of 0.6, the truck can satisfy the requirements of safe operation when passing the 0% bridge damage degree when loading the freight. However, once the bridge damage exceeds 20%, the wheel load shedding rate will significantly increase and cause bridge injury. When the loss is 30%, the wheel load shedding rate of the freight train is 0.633 and the front is 0.582. The difference between the two values is 0.051. When the bridge is damaged by 40%, the wheel load shedding rate of the in-vehicle train is 0.612 and the front is 0.620, which is a difference of 0.008.

As shown in Figure 11(a), the wheel load shedding rate of the passenger train head and passenger train compartment increases with an increase in the bridge damage degree, and the wheel load shedding rate is 20%~40% in the bridge damage. The difference between the two values is substantial. The difference between 0% and 10% and 40% to 50% is relatively minor. The difference in the passenger train in the bridge is 0%~10%, and the difference is 10%~50%. When the damage degree of the bridge is less than or equal to 20%, the weight reduction rate of the front and the passenger train wheels is less than the standard limit of 0.6. The wheel load shedding rate of the passenger train compartment at the bridge damage of 20% is 0.5986. The wheel load shedding rate of the working condition is 0.5608. When the bridge damage degree is 30%, the wheel load shedding rate is 0.6044 and the front wheel load shedding rate is 0.5805. When the bridge damage degree is 40%, the front wheel weight is the load shedding rate of 0.6201 exceeds the weight reduction rate of the car wheel by 0.6106. When the bridge damage degree is 50%, the front wheel weight reduction rate of 0.6284, which is larger than the car wheel weight reduction rate of 0.6176, indicating that the axle load is larger in the bridge injury.

As shown in Figure 11(b), the degree of damage to the bridge increases; the wheel load shedding rate of the truck heads, freight trains, and freightless trains significantly increases; and the growth rate of freight trains with freight is

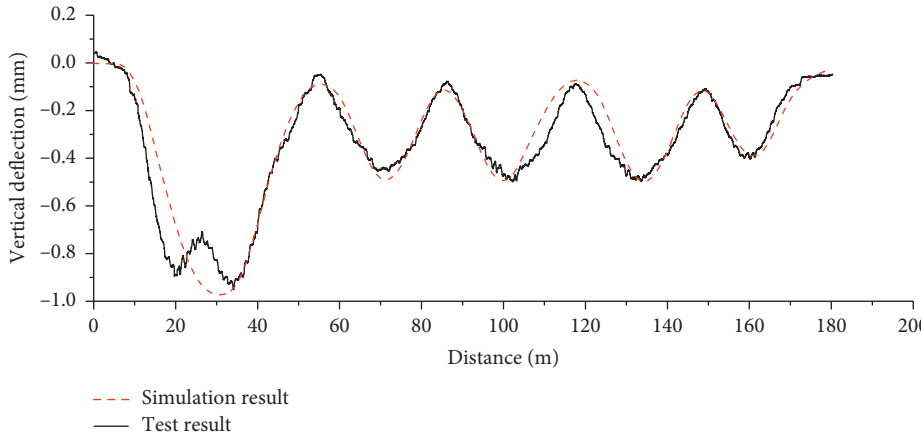

Figure 9: Comparison between field measurement and simulation.

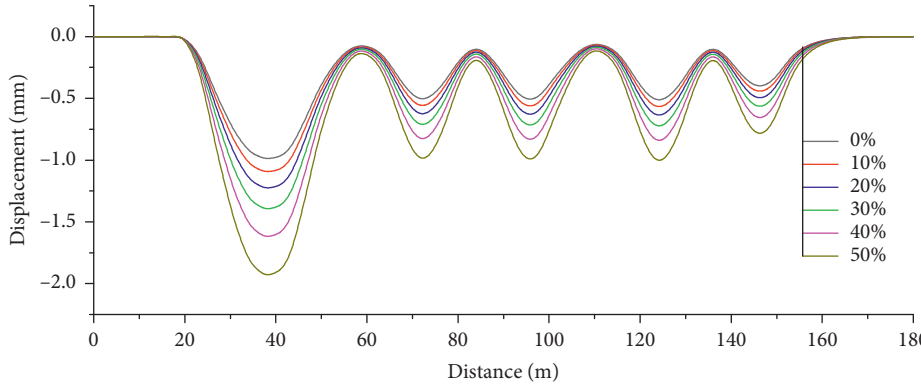

(a)

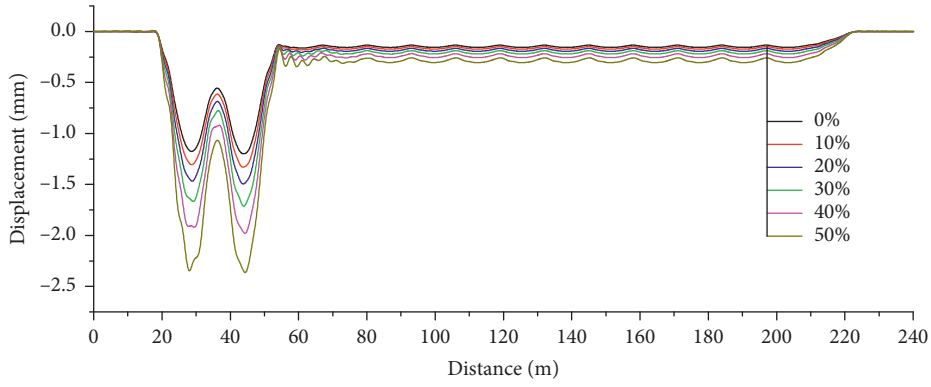

(b)

Figure 10: Continued.

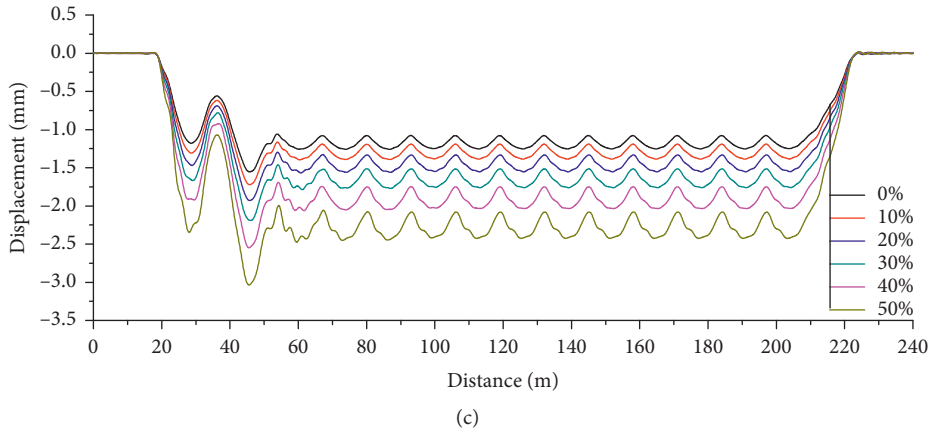

(c)

Figure 10: Vertical displacement response at the mid-span. (a) Passenger train. (b) Freight train (empty). (c) Freight train (cargos).

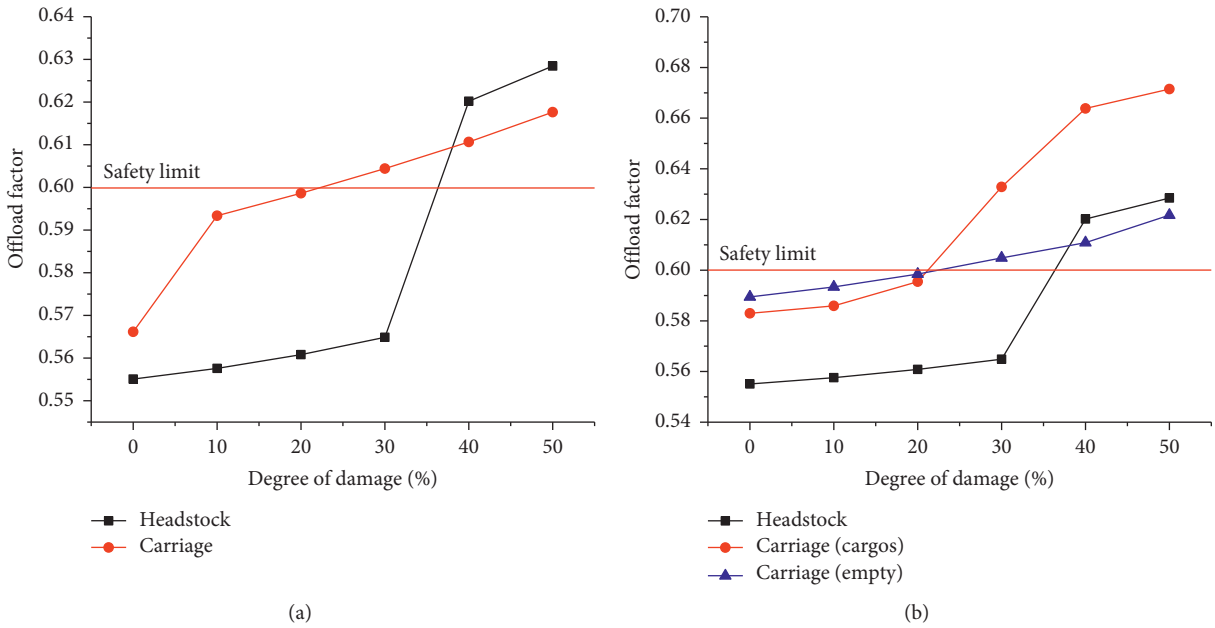

(a) (b)

Figure 11: Rate of wheel load reduction. (a) Passenger train. (b) Freight train.

significantly higher than that of the freightless freight train; that is, the higher the degree of change in the axle load, the heavier the load reduction rate. When the damage degree of the bridge is 20%, standard limits for trucks are 0.5984 and 0.5924. When the bridge damage is 30%, the wheel load shedding rate exceeds the safety limit of 0.6. The truck wheel weight reduction rate is 0.6328, and the truck wheel weight reduction rate is 0.6008, which does not satisfy the operational safety requirements. When the damage degree of the bridge is less than 20%, the weight reduction rate of the front and the two compartments is less than 0.6, which indicates that the bridge has a certain safety reserve in the current state; when the bridge damage is 40%, the wheel load shedding rate exceeds the standard limit. The maximum freight car is 0.6638, the front is 0.6201, and the minimum without freight is 0.6108. This finding is consistent with the results for the axle load. When the bridge damage is 50%, the wheel load shedding rate is 0.6714 for trucks, 0.6284 for cars, and 0.6217 for vans. The weight reduction rate of the in-vehicle train wheel increases with an increase in the bridge damage degree, in which the vehicle body undergoes substantial changes in bridge damage from 20% to 40%, and the wheel body weight reduction rate is always larger than the wheel head wheel weight reduction. The load factor, which is caused by the weight of the truck compartment, is larger than that for the head.

The larger the degree of bridge damage, the higher the wheel load reduction rate, the heavier the vehicle wheel weight, and the larger the wheel load reduction rate.

4.3. Stability of Passenger and Freight Train with Performance Damage of Bridge. This section analyses the stability of the vehicle body with different degrees of performance damage.

The operational stability of passenger and freight trains is examined by considering the maximum acceleration and Sperling's riding index.

4.3.1. Maximum Acceleration of Train Body. As shown in Figure 12, the relationship between the vertical maximum acceleration of the vehicle body and the damage degree of the bridge when the passenger car and the freight train carriage pass through the bridge is analysed. The analysis results indicate that the maximum vertical acceleration of the passenger and freight train crossing bridge does not exceed the limits specified in the specification. The analysis shows that the axle load of the train has a considerable influence on the vertical maximum acceleration of the train. The higher the damage degree of the bridge is, the more distinct the impact of the bridge damage is on the vertical maximum acceleration of the passenger train and the freight train. The damage degree of the four vehicles in the bridge is 50%. The maximum vertical acceleration of the vehicle body that corresponds to 50% is 0.02958 g for the freight car, 0.02013 g for the front, 0.01582 g for the no-car condition, and 0.00777 g for the passenger car. The maximum vertical acceleration of the freight car in the bridge ranges from 0% to 40%, and the average growth rate is 8%. The difference ranges from 40% to 50%, the growth rate is 22.13%, and the passenger train is out of stock when the damage to the bridge is 50%. The maximum vertical acceleration of the vehicle body is 0.00777 g and 0.01582 g, and the growth rate is approximately 13.50%. The maximum vertical acceleration of the front is weak when the bridge is damaged (0%~10%), and the maximum vertical acceleration of the car body is 5.30%, which is relatively flat. When the bridge damage is significant (30%~50%), the maximum vertical acceleration growth rate is 17.51%; when the contrast is lighter, distinct improvements are observed.

The maximum acceleration of the vehicle is considerably affected by the performance degradation of the bridge. The axle load of the vehicle is also affected, but the impact is not as large as the performance degradation of the bridge.

4.3.2. Sperling Index. As shown in Figure 13, the damage to the bridge performance is positively correlated with the Sperling index of trucks and buses. The Sperling index distinctly increased with the damage to the bridge performance. The heavier the wheel, the higher the Sperling index. All values are less than the standard limit of 2.5 and are excellent. The level of bridge damage had a considerable influence on the Sperling index. The Sperling index increased with an increase in the level of bridge damage, which indicates that the comfort level decreased. With an increase in bridge damage, the Sperling index increased, and the degree of increase was distinct. The Sperling index was 1.63, 1.68, 1.74, 1.81, 1.90, and 2.03, and the increments were 0.05, 0.06, 0.07, and 0.09, respectively, when the damage degree of freight trains with goods was 0%, 10%, 20%, 30%, 40%, and 50%, respectively. The Sperling index increment was approximately 0.05~0.09 for each degree of damage.

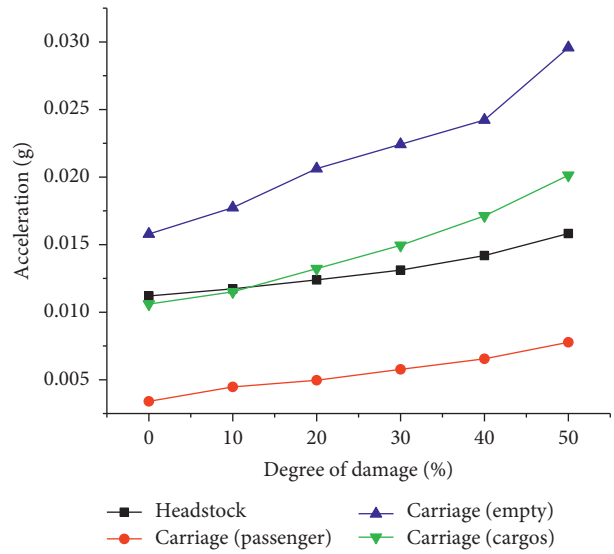

Figure 12: Maximum acceleration of the train body.

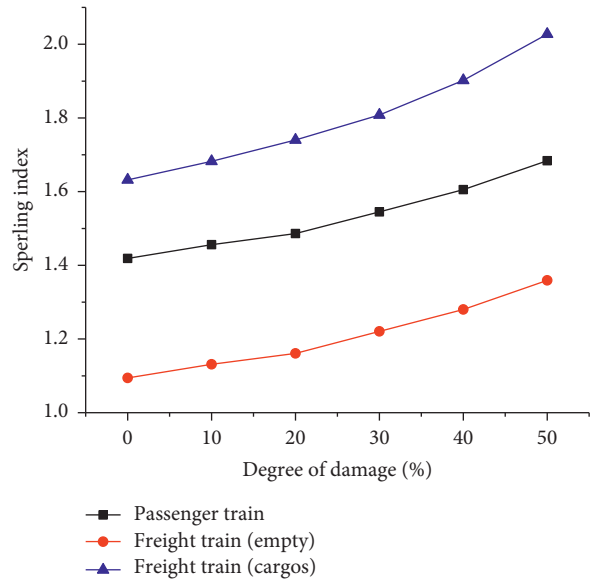

Figure 13: Sperling index.

According to the previous analysis, the effect of bridge performance degradation on the Sperling index is higher than that of the axle weight of the train.

5. Conclusions

(1) The damage of bridge performance is an important factor that affects the safe and stable operation of passenger and freight trains that cross the bridge. With the improvement in bridge performance damage, various indexes (wheel weight reduction rate, maximum vertical acceleration of vehicle body, and Sperling index) that represent passenger and freight train operation safety and stability will increase.

(2) When the DF11 locomotive investigated in this paper is measured on the bridge, the results satisfy the requirement of a safe and smooth bridge crossing with a speed of 60 km/h for passenger and freight trains.

(3) The weight of the body also affects the safety and stability of the freight train that crosses the bridge. With an increase in body weight, the influence of the change in body weight on the safety and stability of a freight train that crosses the bridge will be more distinct.

Data Availability

The data used to support the findings of this study are included within the article.

Disclosure

Kang Liu, Kai Hou, and Zhongyu Fei are co-first authors.

Conflicts of Interest

The authors declare no conflicts of interest.

Authors' Contributions

Kang Liu, Kai Hou, and Zhongyu Fei contributed equally to this work.

Acknowledgments

This study was supported by the China Postdoctoral Science Foundation (2017M622239), the Project of Shandong Province Higher Educational Science and Technology Program (J17KA219), and the National Key Research and Development Program of China (2017YFE9135300).

Supplementary Materials

Supplementary Materials The supplementary materials are the animation of the first-order measured mode-shape. Gif 1 is lateral first-order mode shape, and Gif 2 is vertical first-order mode shape. (*Supplementary Materials*)

References

[1] P. Weston, C. Roberts, G. Yeo, and E. Steswart, "Perspectives on railway track geometry condition monitoring from in-service railway vehicles," *Vehicle System Dynamics*, vol. 53, no. 7, pp. 1063–1091, 2015.

[2] M. Abdollah, P. J. Mcgetrick, and E. J. Obrien, "A review of indirect bridge monitoring using passing vehicles," *Shock and Vibration*, vol. 2015, Article ID 286139, 16 pages, 2015.

[3] A. Alvandi and C. Cremona, "Assessment of vibration-based damage identification techniques," *Journal of Sound and Vibration*, vol. 292, no. 1-2, pp. 179–202, 2006.

[4] Y.-B. Yang, C. W. Lin, and J. D. Yau, "Extracting bridge frequencies from the dynamic response of a passing vehicle," *Journal of Sound and Vibration*, vol. 272, no. 3-5, pp. 471–493, 2004.

[5] Y. B. Yang and C. W. Lin, "Vehicle-bridge interaction dynamics and potential applications," *Journal of Sound and Vibration*, vol. 284, no. 1-2, pp. 205–226, 2005.

[6] C. W. Lin and Y. B. Yang, "Use of a passing vehicle to scan the fundamental bridge frequencies: an experimental verification," *Engineering Structures*, vol. 27, no. 13, pp. 1865–1878, 2005.

[7] P. J. McGetrick, *The Use of an Instrumented Vehicle to Monitor Transport Infrastructure. School of Civil*, Structural and Environmental Engineering, UCD. University College Dublin, Dublin, Ireland, 2012.

[8] C. Gentile and A. Saisi, "Operational modal testing of historic structures at different levels of excitation," *Construction and Building Materials*, vol. 48, pp. 1273–1285, 2013.

[9] A. Bayraktar, T. Türker, and A. C. Altunişik, "Experimental frequencies and damping ratios for historical masonry arch bridges," *Construction and Building Materials*, vol. 75, pp. 234–241, 2015.

[10] L. Dai, L. Wang, M. Deng et al., "Strengthening a 20-year-old post-tensioned concrete box beam with double-layer prestressed steel wire ropes," *Journal of Bridge Engineering*, vol. 23, no. 11, Article ID 05018009, 2018.

[11] L. Li, T. Wu, X. He et al., "Reliability evaluation of vortex-induced vibration for a long-span arch bridge," *Journal of Bridge Engineering*, vol. 23, no. 5, Article ID 05018002, 2018.

[12] W. Li and X. Bian, "Dynamic performance of pile-supported bridge-embankment transition zones under high-speed train moving loads," *Procedia Engineering*, vol. 143, pp. 1059–1067, 2016.

[13] J. Mao, Z. Yu, Y. Xiao, C. Jin, and Y. Bai, "Random dynamic analysis of a train-bridge coupled system involving random system parameters based on probability density evolution method," *Probabilistic Engineering Mechanics*, vol. 46, pp. 48–61, 2016.

[14] T. Real, C. Zamorano, C. Hernández, J. A. García, and J. I. Real, "Static and dynamic behavior of transitions between different railway track typologies," *KSCE Journal of Civil Engineering*, vol. 20, no. 4, pp. 1356–1364, 2016.

[15] D. Ulgen, O. L. Ertugrul, and M. Y. Ozkan, "Measurement of ground borne vibrations for foundation design and vibration isolation of a high-precision instrument," *Measurement*, vol. 93, pp. 385–396, 2016.

[16] C. A. Ribeiro, R. Calçada, and R. Delgado, "Experimental assessment of the dynamic behaviour of the train-track system at a culvert transition zone," *Engineering Structures*, vol. 138, pp. 215–228, 2017.

[17] J. N. Varandas, A. Paixão, and E. Fortunato, "A study on the dynamic train-track interaction over cut-fill transitions on buried culverts," *Computers & Structures*, vol. 189, pp. 49–61, 2017.

[18] M. A. Sayed, M. R. Kaloop, E. Kim, and D. Kim, "Assessment of acceleration responses of a railway bridge using wavelet analysis," *KSCE Journal of Civil Engineering*, vol. 21, no. 5, pp. 1844–1853, 2017.

[19] X.-Z. Li, J. Xiao, D.-J. Liu, M. Wang, and D.-Y. Zhang, "An analytical model for the fluctuating wind velocity spectra of a moving vehiclefluctuating wind velocity spectra of a moving vehicle," *Journal of Wind Engineering and Industrial Aerodynamics*, vol. 164, pp. 34–43, 2017.

[20] X. Li, Q. Liu, S. Pei, L. Song, and X. Zhang, "Structure-borne noise of railway composite bridge: numerical simulation and experimental validation," *Journal of Sound and Vibration*, vol. 353, pp. 378–394, 2015.

[21] S. J. Wang, Z. D. Xu, S. Li, and S. J. Dyke, "Safety and stability of light-rail train running on multispan bridges with deformation," *Journal of Bridge Engineering*, vol. 21, no. 9, Article ID 06016004, 2016.

[22] X. Wu, M. Chi, and H. Gao, "Post-derailment dynamic behaviour of a high-speed train under earthquake excitations," *Engineering Failure Analysis*, vol. 64, pp. 97–110, 2016.

[23] N. Lestoille, C. Soize, and C. Funfschilling, "Stochastic prediction of high-speed train dynamics to long-term evolution of track irregularities," *Mechanics Research Communications*, vol. 75, pp. 29–39, 2016.

[24] L. Deng and W. C. Yan, "Vehicle weight limits and overload permit checking considering the cumulative fatigue damage of bridges," *Journal of Bridge Engineering*, vol. 23, no. 7, Article ID 04018045, 2018.

[25] S. Tan, Z. Yu, Z. Shan, and J. Mao, "Influences of train speed and concrete Young's modulus on random responses of a 3D train-track-girder-pier coupled system investigated by using PEM," *European Journal of Mechanics—A/Solids*, vol. 74, pp. 297–316, 2019.

[26] A. H. Almasri and Q. F. Al-Waked, "Inspection and numerical analysis of an ottoman railway bridge in Jordan," *Advances in Materials Science and Engineering*, vol. 2016, Article ID 9039483, 7 pages, 2016.

[27] L. N. Zhang, F. C. Li, X. Yu, P. F. Cui, and X. Y. Wang, "Experimental research on 2: 1 parametric vibration of stay cable model under support excitation," *Advances in Materials Science and Engineering*, vol. 2016, Article ID 9804159, 9 pages, 2016.

[28] H. L. Li, D. M. Frangopol, M. Soliman, and H. Xia, "Fatigue reliability assessment of railway bridges based on probabilistic dynamic analysis of a coupled train-bridge system," *Journal of Structural Engineering*, vol. 142, no. 3, Article ID 04015158, 2015.

[29] A. Morassi and S. Tonon, "Dynamic testing for structural identification of a bridge," *Journal of Bridge Engineering*, vol. 13, no. 6, pp. 573–585, 2008.

[30] G. Zanardo, H. Hao, Y. Xia, and A. J. Deeks, "Stiffness assessment through modal analysis of an RC slab bridge before and after strengthening," *Journal of Bridge Engineering*, vol. 11, no. 5, pp. 590–601, 2006.

[31] National Standard of the People's Republic of China, *Railway Transport (2004) No. 120 Railway Bridge Verification Specification*, China Railway Publishing House, Beijing, China, 2004.

[32] X. Z. Li, H. J. Lei, and Y. Zhu, "Analysis of Rayleigh damping parameters in a dynamic system of vehicle-track-bridge," *Journal of Vibration and Shock*, vol. 32, pp. 52–57, 2015.

[33] K. C. Anil, *University of California at Berkeley, Dynamics of Structures*, Pearson, London, UK, 4th edition, 2011.

[34] M. Majka and M. Hartnett, "Effects of speed, load and damping on the dynamic response of railway bridges and vehicles," *Computers & Structures*, vol. 86, no. 6, pp. 556–572, 2008.

[35] M. Majka and M. Hartnett, "Dynamic response of bridges to moving trains: a study on effects of random track irregularities and bridge skewness," *Computers & Structures*, vol. 87, no. 19-20, pp. 1233–1252, 2009.

[36] J. Lemaitre, "How to use damage mechanics," *Nuclear Engineering and Design*, vol. 80, no. 2, pp. 233–245, 1984.

[37] J. Lemaitre and J. Dufailly, "Damage measurements," *Engineering Fracture Mechanics*, vol. 28, no. 5-6, pp. 643–661, 1987.